Ab initio treatment of charge transfer in ion-molecule collisions based on one-electron wave functions

P. M. M. Gabás,* L. F. Errea, L. Méndez, and I. Rabadán†

Laboratorio Asociado al CIEMAT de Física Atómica y Molecular en Plasmas de Fusión, Departamento de Química, Universidad Autónoma de Madrid, Madrid ES-28049, Spain

(Received 4 November 2011; published 11 January 2012)

Two simple *ab initio* methods based on one-electron wave functions are employed to calculate the single-electron capture and single ionization of H_2O and CO molecules by ion impact. The anisotropy of the molecular targets is taken into account by using multicenter pseudopotentials to represent the interaction of the active electron with the ionic molecular core. These two methods are applied to the study of three collisional systems: $H^+ + H_2O$, $He^{2+} + H_2O$, and $C^{2+} + CO$. Comparison with experiments and other theoretical works is presented when available.

DOI: 10.1103/PhysRevA.85.012702 PACS number(s): 34.70.+e, 34.50.−s

I. INTRODUCTION

Collisions between ions and molecules are relevant processes in cold plasmas, which have motivated a large amount of experimental [1–7] and theoretical [8–12] works.

Although, for small molecules, *ab initio* electronic structure calculations can be performed with high accuracy, complex systems require expensive computational resources. Moreover, dynamical calculations for these systems demand simplified methods that avoid the need to regularize the divergent behavior of dynamical couplings at conical intersections, regions where potential energy surfaces cross, and where nonadiabatic transitions predominantly take place (see, e.g., [13] and references therein).

We present two simple semiclassical *ab initio* methods to study collisions with polyatomic molecules. In this work, we have focused on the evaluation of single-electron capture (SEC) and single ionization (SI) processes:

$$P^+ + T \longrightarrow P + T^+ \quad \text{(SEC)}, \tag{1}$$

$$P^+ + T \longrightarrow P^+ + T^+ + e^- \quad \text{(SI)}, \tag{2}$$

where P represents the projectile (H^+, He^{2+}, or C^{2+}) and T the target (H_2O or CO). In the next section, we describe the main details of the two approaches employed, which are based on the use of a multicenter pseudopotential to account for the interaction of the active electron with the multielectronic and/or polyatomic target and projectile. Also, the independent particle model (IPM) is used to define either transition probabilities or to simplify the evaluation of matrix elements between multielectronic states.

CO and H_2O are the second- and third-most abundant molecules in the universe, respectively [14]. This makes the information about their molecular structure and dynamical aspects essential for astrophysical purposes. Both of them play important roles for life, too; water is a dominant component in cells (see, e.g., [15]), and CO plays a fundamental role in the human body as a signaling molecule (most probably a neurotransmitter; see [16]); it also appears as a secondary product after DNA chain damage [8]. In particular, given the scarce information available in the literature, the study of the interaction of carbon ions [17–19] as C^{2+} with CO molecules is of great importance.

As shown in previous works [20], charge transfer shows a marked anisotropy with respect to target-projectile relative orientation; therefore, we perform calculations for several collisional orientations.

In this work, all calculations have been performed in the laboratory reference frame (LRF). This choice is justified by the important simplification obtained in the structural calculations, avoiding the need to reorient the target molecule as the projectile moves in the collisional trajectory. Moreover, evaluation of the dynamical couplings, electronic energies, and corrections due to the introduction of a common translation factor (CTF) [21] also becomes easier in the LRF.

Dynamical calculations are performed in a wide energy range covering from 0.1 to 110 keV. The symbols a_0 and E_h are used to refer to the atomic units of length and energy, respectively.

II. THEORETICAL METHODS

Within the semiclassical eikonal *ab initio* approach [22], we assume that the projectile follows straight-line trajectories with impact parameter **b** and velocity **v**:

$$\mathbf{R}(t) = \mathbf{b} + \mathbf{v}t, \tag{3}$$

adequate for $E > 100$ eV, where most of the experiments are carried out.

A. Asymptotic molecular orbitals and pseudopotentials

The presence of conical intersections (CIs) between adiabatic electronic molecular states is a well-known feature of *ab initio* treatment of ion-molecule collisions. At the loci of the CI, the adiabatic wave functions present singular, nonintegrable couplings that must be removed prior to any dynamical treatment. A rigorous formalism to perform this regularization was presented in Ref. [13]. Nevertheless, if the number of CIs to be regularized is large, it is more practical to use nonadiabatic electronic states given that the couplings between them behave smoothly even at the loci of the CI.

Therefore, in this work the scattering wave function is expanded in terms of nonadiabatic molecular orbitals (MOs), $\phi(R)$, obtained from asymptotic orbitals, solutions of the eigenvalue equation at a very large value of the projectile-target

*pablo.martinez.martinez@uam.es
†ismanuel.rabadan@uam.es

distance $R_a = 1000a_0$:

$$h(\mathbf{r}; R_a)\phi_i(R_a) = \epsilon_i\phi_i(R_a), \tag{4}$$

where $h(\mathbf{r}; R_a)$ is the fixed-nuclei Hamiltonian given by

$$h(\mathbf{r}; R_a) = -\tfrac{1}{2}\nabla^2 + V_{\mathrm{T}^+} + V_{\mathrm{P}}, \tag{5}$$

where V_{T^+} is the electron-target interaction potential and V_{P} is the electron-projectile one. The ϕ orbitals reflect the separated projectile and target electronic structure.

Equation (4) is solved in a large GTO basis sets $\{\xi\}$. We have used the one provided by Widmark *et al.* [23] to describe the water hydrogen atoms in $H^+ + H_2O$ and $He^{2+} + H_2O$ systems and both molecular and ion carbon atoms in the $C^{2+} + CO$ system. For the proton projectile in the $H^+ + H_2O$ system we have used the basis set provided in Ref. [24]; for He we have optimized the basis set available in Ref. [25] and for the oxygen atom in all the systems we have used the basis set given in Ref. [26].

For a large internuclear distance ($R_a \approx 1000a_0$), the solution of the Schrödinger equation (4) provides the (asymptotic) coefficient matrix $\mathbf{C}(R_a)$:

$$\phi_i(R_a) = \sum_j c_{ij}(R_a)\xi_j(R_a), \tag{6}$$

which is employed to construct the MOs ϕ_i at any other internuclear position $\mathbf{R}$,

$$\phi_i(\mathbf{R}) = \sum_j c_{ij}(R_a)\xi_j(\mathbf{R}). \tag{7}$$

In this work, the basis set $\{\phi_i(\mathbf{R})\}$ for the $H^+ + H_2O$ system contains 108 MOs, 5 of which are water MOs, 78 describe ionization, 6 account for projectile electron capture, and 19 correspond to target excitation. In the $He^{2+} + H_2O$ system we have 130 MOs, 5 of which are water valence orbitals, 85 describe ionization, 18 are projectile electron capture, and 22 represent target excitation orbitals. With respect to $C^{2+} + CO$, we have obtained a total of 185 MOs, of which 7 are CO MOs, 2 represent C^{2+} passive doubly occupied orbitals, 135 have positive energy, 15 account for projectile electron capture and 26 correspond to target excitation.

In Eq. (5), V_{T^+} is a multicenter pseudopotential representing the interaction of the active electron with the molecular ion (H_2O^+ or CO^+), and V_{P^+} is the Coulomb potential in the case of H^+ and He^{2+} projectiles and a pseudopotential for C^{2+}. The expressions of these pseudopotentials are

$$V_{H_2O^+}(r_O, r_{H_1}, r_{H_2}) = V_O(r_O) + V_H(r_{H_1}) + V_H(r_{H_2}), \tag{8}$$

$$V_{CO^+}(r_O, r_C) = V_O(r_O) + V_C(r_C), \tag{9}$$

with

$$V_k = -\frac{N_A - N_k}{r_k} - \frac{N_k}{r_k}(1 + \alpha_k r_k)e^{-2\alpha_k r_k}|s\rangle\langle s| - \gamma_k \frac{N_k}{r_k}(1 + \tau_k r_k)\, e^{-2\tau_k r_k}[1 - |s\rangle\langle s|], \tag{10}$$

where N_A is the atomic number of the corresponding atom A, N_k is the screening charge of the atom k, and r_k is the distance between the active electron and the atom k. These expressions contain free parameters which have been fitted to minimize the difference between the energies of the orbitals in the pseudopotential with the energies of the same orbitals in a self-consistent field (SCF) calculation of the system, with final differences after the fitting procedure smaller than $4 \times 10^{-3} E_h$ for each valence orbital. The values of the fitted parameters are given in Table I. Derived parameters from the fitted ones are $N_H = (9 - N_O)/2$ (for H_2O^+) and $N_C = 13 - N_O$ (for CO^+). In Table II, the energies obtained with the pseudopotential calculation are compared with the SCF ones using the same basis sets and it can be seen that there is a general good agreement between them.

TABLE I. Fitted parameters for the different target and projectile pseudo potentials. The units of α_k and τ_k are ${a_0}^{-1}$.

Parameters	H_2O^+	CO^+	C^{2+}
N_O	7.162	7.609	
α_O	1.480	1.501	
τ_O	1.600	1.503	
γ_O	1	1	
α_H	0.665		
γ_H	0		
N_H	$(9 - N_O)/2$		
α_C		0.850	0.963
τ_C		1.020	1.451
γ_C		1	1
N_C		$13 - N_O$	4

B. Method I (MI)

In this method, the one-electron scattering wave function is a solution of the time-dependent Schrödinger equation,

$$\left(h - i\frac{\partial}{\partial t}\right)\Psi_{\mathrm{MI}}(\mathbf{r}, t) = 0, \tag{11}$$

with the Hamiltonian given in Eq. (5).

Using the molecular basis set $\{\phi\}$ of Eq. (7), the dynamical one-electron wave function Ψ_{MI} is expanded as

$$\Psi_{\mathrm{MI}}(\mathbf{r}; t) = \sum_j a_j(t)\phi_j \exp\left(-i\int_0^t dt'\,\lambda_j\right), \tag{12}$$

where $\lambda_j = (\mathbf{s}^{-1}\mathbf{h})_{jj}$ and where $\mathbf{s}$ and $\mathbf{h}$ are the overlap and Hamiltonian matrices in the basis $\{\phi\}$.

TABLE II. Fitted pseudopotential and SCF energies (in E_h) of the valence orbitals for H_2O, CO, and C^{2+} systems.

Orbitals	$2a_1$	$1b_2$	$3a_1$	$1b_1$
H_2O (SCF)	−1.3503	−0.721 73	−0.584 96	−0.510 79
H_2O (pseudo)	−1.3556	−0.720 67	−0.588 18	−0.513 81
Orbitals	σ_{2s}	σ^*_{2s}	π_{2p}	σ_{2p}
CO (SCF)	−1.518 51	−0.804 09	−0.638 40	−0.555 44
CO (pseudo)	−1.461 79	−0.860 78	−0.638 42	−0.558 39
Orbitals	$2s$			
C^{2+} (SCF)	−1.694 05			
C^{2+} (pseudo)	−1.693 46			

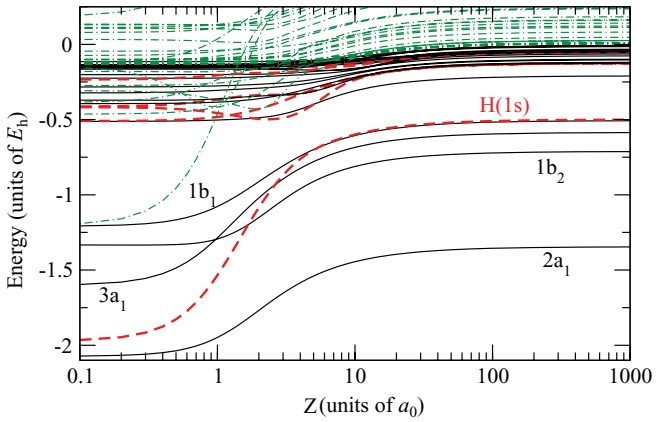

FIG. 1. (Color online) Diagonal Hamiltonian matrix elements of $\mathbf{h}_{\rm MI}$ obtained in the basis $\{\phi\}$ for the $H^+ + H_2O$ system along the trajectory t_1 with impact parameter $b = 1a_0$. Solid and dashed lines correspond to MOs with asymptotic negative energy and located on the target and the projectile, respectively, while dot-dashed lines correspond to MOs with asymptotic positive energy.

In Fig. 1, we show the diagonal matrix elements of the Hamiltonian $\mathbf{h}$ as a function of the projectile position along a specific projectile trajectory t_1 [plotted in Figs. 2(a) and 3] in $H^+ + H_2O$ collisions with an impact parameter $b = 1a_0$. The dashed lines correspond to MOs that asymptotically describe SEC; the solid lines correspond to MOs that asymptotically represent a bound electron into the H_2O^+ pseudopotential, and dot-dashed lines come from molecular pseudostates with asymptotic positive energy; their population account for an estimate of the ionization cross section.

The substitution of expansion (12) into the time-dependent Schrödinger equation (11) leads to a system of first-order differential equations:

$$i\frac{da_i}{dt} = \sum_k (\mathbf{s}^{-1}\mathbf{M})_{ik} a_k, \tag{13}$$

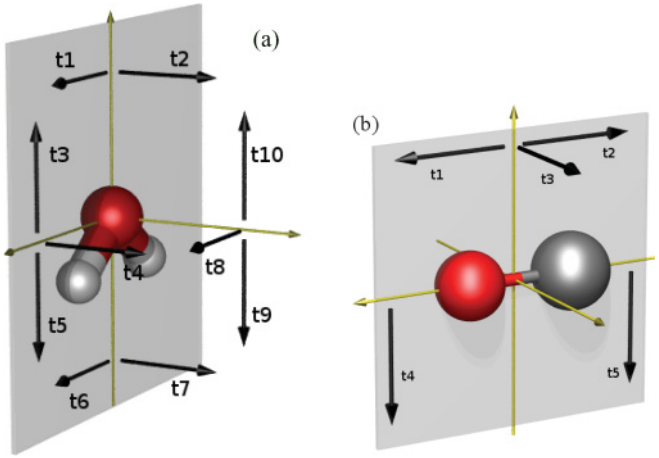

FIG. 2. (Color online) Diagrams of the ten and five trajectories detailed in Table IV used in studying (a) $[H^+,He^{2+}] + H_2O$ and (b) $C^{2+} + CO$ collisions, respectively.

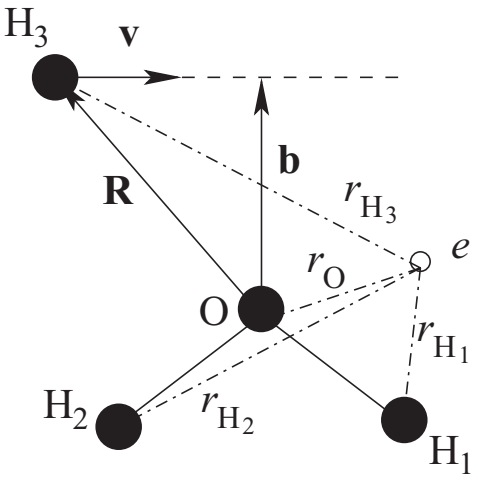

FIG. 3. Projectile trajectory t_1 in $H^+ + H_2O$ collisions with indication of distances.

where the coupling matrix elements are

$$M_{ik} = \langle\phi_i|h - i\frac{\partial}{\partial t}|\phi_k\rangle. \tag{14}$$

Equation (13) is solved along each projectile trajectory $\mathbf{R}(t)$ and each initial condition that assumes that the active electron is initially in one of the valence MOs of the target molecule (e.g., for water): $a_j(t=0) = \delta_{ij}$, with $j = 2,3,4,5$ representing $2a_1$, $1b_2$, $3a_1$, and $1b_1$ MOs, respectively. The one-electron transition probability from ϕ_j to ϕ_i along a given trajectory is

$$p_{ij} = |\langle\Psi_{\rm MI}(R_a)|\phi_i(R_a)\rangle|^2 = |a_i(R_a)|^2. \tag{15}$$

According to this expression, monoelectronic capture, $p_j^{\rm sec}$, and ionization, $p_j^{\rm ion}$, probabilities from the orbital ϕ_j are given by

$$p_j^{\rm sec} = \sum_i p_{ij} \quad \text{if} \quad \epsilon_i(R_a) < 0 \quad \text{with orbital}$$
$$i \quad \text{located on the projectile}, \tag{16}$$

$$p_j^{\rm ion} = \sum_i p_{ij} \quad \text{if} \quad \epsilon_i(R_a) > 0. \tag{17}$$

Multielectron probabilities are obtained from these (pseudopotential) probabilities by using the independent event model (IEVM) [27,28]:

$$P^{\rm SEC} = 2\sum_j p_j^{\rm sec}\left(1 - p_j^{\rm ion} - p_j^{\rm sec}\right), \tag{18}$$

$$P^{\rm ION} = 2\sum_j p_j^{\rm ion}\left(1 - p_j^{\rm ion} - p_j^{\rm sec}\right), \tag{19}$$

with j running over target valence MO.

C. Method II (MII)

In this method, the scattering wave function, $\Psi_{\rm MII}$, is expanded in terms of configurations $\{\Phi_i\}$ built using the set of asymptotic MOs $\{\phi_i\}$ of Eq. (7). The set of configurations $\{\Phi_i\}$ includes one that represents the entrance channel $P^{q+} + T$ for projectiles H^+, He^{2+}, or C^{2+} and targets H_2O and CO,

with the target in its ground electronic state. The exit channel configurations are obtained as single excitations from the ground-state configuration:

$$\Phi_1 = ||\phi_1\bar{\phi}_1 \ldots \phi_n\bar{\phi}_n|| \quad \text{entrance channel}, \tag{20}$$

$$\Phi_j = ||\phi_1\bar{\phi}_1 \ldots \phi_m\bar{\phi}_l|| + ||\phi_1\bar{\phi}_1 \ldots \phi_l\bar{\phi}_m|| \quad \text{exit channels}, \tag{21}$$

where m runs over the occupied MOs of the target and l labels one of the unoccupied orbitals of the collisional system (see the Appendix for more detailed information). If ϕ_l is a target orbital, the configuration represents an excitation, if ϕ_l is a projectile orbital, it corresponds to electron capture; if the energy of ϕ_l is positive, the transition to the corresponding configuration is interpreted as ionization.

The collisional wave function is expanded in the set of configurations of Eqs. (20) and (21) as

$$\Psi_{\text{MII}}(\mathbf{r};t) = \sum_j d_j(t)\Phi_j \exp\left(-i\int_0^t dt'\Lambda_j\right), \tag{22}$$

where $\mathbf{r}$ denotes the electronic coordinates, while $\Lambda_j = (\mathbf{S}^{-1}\mathbf{H})_{jj}$, with $\mathbf{S}$ and $\mathbf{H}$ the overlap and MII-Hamiltonian matrices in the basis $\{\Phi\}$. Using this wave function as solution of the dynamical equation

$$\left(H - i\frac{\partial}{\partial t}\right)\Psi_{\text{MII}}(\mathbf{r},t) = 0, \tag{23}$$

we obtain the transition probability from the entrance channel Φ_1 to the state Φ_i, for a given trajectory m, by integrating a system of coupled differential equations similar to that of Eq. (13):

$$P_{m,i} = |\langle\Psi_{\text{MII}}(R_a)|\Phi_i(R_a)\rangle|^2 = |d_i(R_a)|^2. \tag{24}$$

In particular, the SEC and SI probabilities are

$$P_m^{\text{SEC}} = \sum_k P_k; \quad P_m^{\text{SI}} = \sum_l P_l, \tag{25}$$

where the index k runs over configurations representing electron capture and the index l labels configurations that contain an excitation to a MO with positive energy.

In this method we solve the eikonal equation for a multielectronic wave function and, consequently, there is no need for an independent-particle interpretation of the probabilities because they are directly obtained from Eq. (24). On the other hand, the method requires the evaluation of two-electron integrals. To simplify this task, we have employed the IPM [29] to approximate the evaluation of the Hamiltonian matrix elements in the configuration basis set:

$$\langle\Phi_i|H|\Phi_j\rangle \approx \langle\Phi_i|\sum_{j=1}^{2n} h|\Phi_j\rangle, \tag{26}$$

where $2n$ is the total number of electrons.

D. Common translation factor

Common translation factors have been extensively employed in previous ion-atom and ion-diatom collisional studies (see, for example, [30,31]) to ensure that a truncated expansion of the scattering wave function fulfills the boundary conditions of the system and preserve the Galilean invariance of the results. The use of a velocity field (or CTF) has been shown to be one of the most practical choices, as a correction to potential or dynamical couplings can still be written without explicit plane-wave functions in the integrands. In this work, we solve the time-dependent Schrödinger equation along the projectile trajectory in the LRF for a wave function Ψ^{CTF},

$$\left(H - i\frac{\partial}{\partial t}\right)\Psi^{\text{CTF}} = 0, \tag{27}$$

that includes a CTF [32],

$$\Psi^{\text{CTF}} = e^{iU(\mathbf{r},t)}\Psi \equiv D\Psi, \tag{28}$$

with

$$U(\mathbf{r},t) = f(\mathbf{r},t)\mathbf{v}\mathbf{r} - \tfrac{1}{2}f^2(\mathbf{r},t)v^2t, \tag{29}$$

where $f(\mathbf{r},t)$ is a switching function that depends on both the electronic coordinates, $\mathbf{r}$, and the time-dependent nuclear position, $R(t)$:

$$f(\mathbf{r},t) = g(R)\left[\frac{b}{R}x + \frac{vt}{R}z\right], \tag{30}$$

which contains a cutoff function of the form

$$g(R) = \frac{R}{R^2+\eta^2}, \tag{31}$$

where η refers to the range of internuclear distances where corrections due to the introduction of a CTF become very small. The matrix elements arising from Eq. (27) are calculated as

$$\begin{aligned}\left\langle\Psi_i^{\text{CTF}}\middle|H - i\frac{\partial}{\partial t}\middle|\Psi_j^{\text{CTF}}\right\rangle &= \epsilon_j\delta_{ij} + \langle\Psi_i|-i\frac{\partial}{\partial t}|\Psi_j\rangle \\ &+ \langle\Psi_i|-\frac{1}{2}i\sum_{l=1}^{N}\nabla_l^2U - i\sum_{l=1}^{N}\nabla_lU\nabla_l|\Psi_j\rangle \\ &+ \langle\Psi_i|\frac{\partial U}{\partial t} - \frac{1}{2}\sum_{l=1}^{N}(\nabla_lU)^2|\Psi_j\rangle,\end{aligned} \tag{32}$$

with N the total number of valence electrons.

We have verified that terms proportional to v^2 appearing in the couplings coming from the introduction of this CTF (29) lead to the overestimation of the SEC cross sections at intermediate collisional velocities ($v > 1$ a.u.). This effect, previously described in ion-atom collisions (see [21]), can be attributed to the singular behavior of the specific form of the switching function $f(r,R)$ at very small values of R. In these situations, the cutoff parameter η can be employed to (almost) suppress the unphysical effect of these terms in the region of small internuclear distances R, where the basis is complete to practical purposes. According to this behavior, we have used larger values of η as the energy of the collision increases.

Given the very large (almost complete) asymptotic MO basis sets $\{\phi\}$ employed in MI, we have not introduced any translation factor (TF) in this method.

E. Anisotropy and orientation-averaged cross sections

Single-electron capture and ionization probabilities, hence cross sections, are calculated along the specific projectile trajectory defined in the LRF which, in the eikonal approximation, follows the classical trajectory $\mathbf{R} = \mathbf{b} + \mathbf{v}t$. By fixing the direction of $\hat{\mathbf{v}}$ in the LRF, say $\hat{\mathbf{z}}$, the relative orientation of the target molecule can be determined by the three Euler angles α,β,γ [33]. The average over all possible target orientations produces orientation-averaged cross sections that can be compared with experimental data:

$$\bar{\sigma}(v) = \frac{1}{4\pi}\int_0^\infty db\, b \int_0^{2\pi} d\alpha \int_0^{\pi} d\beta\, \sin\beta \times \int_0^{2\pi} d\gamma\, P(b,v,\alpha,\beta,\gamma). \tag{33}$$

The integrals over the Euler angles can be calculated using quadrature methods; in particular, we employ the 24-point formula obtained by taking equally spaced points in the angle variables in increments of $\pi/2$ and removing repetitions

$$(\alpha_i,\beta_j,\gamma_j) = \{\alpha_i \otimes (\beta,\gamma)_j\} \quad i = 1,\ldots,4; \quad j = 1,\ldots,6, \tag{34}$$

with

$$\begin{aligned} \alpha_i &\in \{0,\pi/2,\pi,3\pi/2\}, \\ (\beta,\gamma)_j &\in \{(0,0),(\pi/2,0),(\pi/2,\pi/2),(\pi/2,\pi), \\ &\quad (\pi/2,3\pi/2),(\pi,0)\}. \end{aligned} \tag{35}$$

The orientations of the target molecule with respect to the projectile trajectory can be equivalently accounted for by fixing the molecule in the LRF and varying the orientation of $\hat{\mathbf{b}}$ and $\hat{\mathbf{v}}$, with the restriction of $\hat{\mathbf{b}} \perp \hat{\mathbf{v}}$. The 24 points are equivalently described with the pairs detailed in Table III.

We can take advantage of the molecular symmetries to reduce the number of projectile trajectories that are actually different. For example, if the water molecule is in the XZ plane, with the C_2 axis along $\hat{\mathbf{z}}$, collisional orientations 21 and 22 (see Table III) are equivalent and only one of them needs to be explicitly calculated. This argument makes it possible to reduce the number of orientations to be calculated in ion collisions with the water molecule, in its equilibrium geometry, from 24 to 10, which are those indicated in Fig. 2(a). For the CO molecule, given its higher symmetry, from the 24 initial orientations, only the five detailed in Fig. 2(b) need to be calculated. The 24 orientations are detailed in Table III.

TABLE III. Pairs of unitary impact parameter and velocity vectors $(\hat{\mathbf{b}},\hat{\mathbf{v}})_i$ employed to determine collisional projectile orientations.

i	$(\hat{\mathbf{b}},\hat{\mathbf{v}})_i$	i	$(\hat{\mathbf{b}},\hat{\mathbf{v}})_i$	i	$(\hat{\mathbf{b}},\hat{\mathbf{v}})_i$	i	$(\hat{\mathbf{b}},\hat{\mathbf{v}})_i$
1	$(\hat{\mathbf{x}},\hat{\mathbf{y}})$	2	$(\hat{\mathbf{x}},-\hat{\mathbf{y}})$	3	$(\hat{\mathbf{x}},\hat{\mathbf{z}})$	4	$(\hat{\mathbf{x}},-\hat{\mathbf{z}})$
5	$(-\hat{\mathbf{x}},\hat{\mathbf{y}})$	6	$(-\hat{\mathbf{x}},-\hat{\mathbf{y}})$	7	$(-\hat{\mathbf{x}},\hat{\mathbf{z}})$	8	$(-\hat{\mathbf{x}},-\hat{\mathbf{z}})$
9	$(\hat{\mathbf{y}},\hat{\mathbf{x}})$	10	$(\hat{\mathbf{y}},-\hat{\mathbf{x}})$	11	$(\hat{\mathbf{y}},\hat{\mathbf{z}})$	12	$(\hat{\mathbf{y}},-\hat{\mathbf{z}})$
13	$(-\hat{\mathbf{y}},\hat{\mathbf{x}})$	14	$(-\hat{\mathbf{y}},-\hat{\mathbf{x}})$	15	$(-\hat{\mathbf{y}},\hat{\mathbf{z}})$	16	$(-\hat{\mathbf{y}},-\hat{\mathbf{z}})$
17	$(\hat{\mathbf{z}},\hat{\mathbf{x}})$	18	$(\hat{\mathbf{z}},-\hat{\mathbf{x}})$	19	$(\hat{\mathbf{z}},\hat{\mathbf{y}})$	20	$(\hat{\mathbf{z}},-\hat{\mathbf{y}})$
21	$(-\hat{\mathbf{z}},\hat{\mathbf{x}})$	22	$(-\hat{\mathbf{z}},-\hat{\mathbf{x}})$	23	$(-\hat{\mathbf{z}},\hat{\mathbf{y}})$	24	$(-\hat{\mathbf{z}},-\hat{\mathbf{y}})$

TABLE IV. Relation between the trajectory names used in this paper and their spatial orientation detailed in Table III.

H_2O	CO
t_1: 17, 18	t_1: 17, 21, 9, 13
t_2: 19, 20	t_2: 18, 22, 10, 14
t_3: 3, 7	t_3: 19, 20, 23, 24, 11, 12, 15, 16
t_4: 1, 2, 5, 6	t_4: 1, 2, 3, 4
t_5: 4, 8	t_5: 5, 6, 7, 8
t_6: 21, 22	
t_7: 23, 24	
t_8: 9, 10, 13, 14	
t_9: 12, 16	
t_{10}: 11, 15	

Table IV details the labeling of the trajectories we have employed in this work for both H_2O and CO targets.

In summary, the evaluation of orientation-averaged cross sections for the equilibrium geometry of the water molecule oriented as in Fig. 2(a) is obtained as

$$\sigma = \frac{1}{12}\left(\sum_{t=1}^{10}\sigma_t + \sigma_4 + \sigma_8\right), \tag{36}$$

and, in the case of the CO target [Fig. 2(b)]:

$$\sigma = \frac{1}{6}\left(\sum_{t=1}^{5}\sigma_t + \sigma_3\right). \tag{37}$$

To illustrate the influence of the trajectory orientation in the SEC cross sections, we plot in Fig. 4 the results obtained for $H^+ + H_2O$ collisions for the ten trajectory types indicated in Fig. 2(a). It can be observed that the SEC cross sections strongly depend on the orientation of the trajectory. The orientation-averaged SEC cross section [Eq. (36)] is also included.

In Fig. 5 we show the capture probabilities $bP(b)$ as a function of the impact parameter b for three orientations

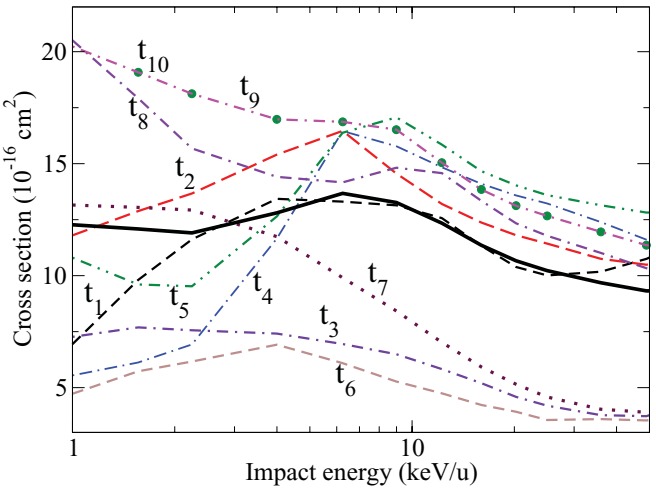

FIG. 4. (Color online) SEC cross section in $H^+ + H_2O$ collisions, for the ten trajectories depicted in Fig. 2(a), calculated with MII and cutoff parameter $\eta = 2$. The solid line is the orientation-averaged result obtained with Eq. (36).

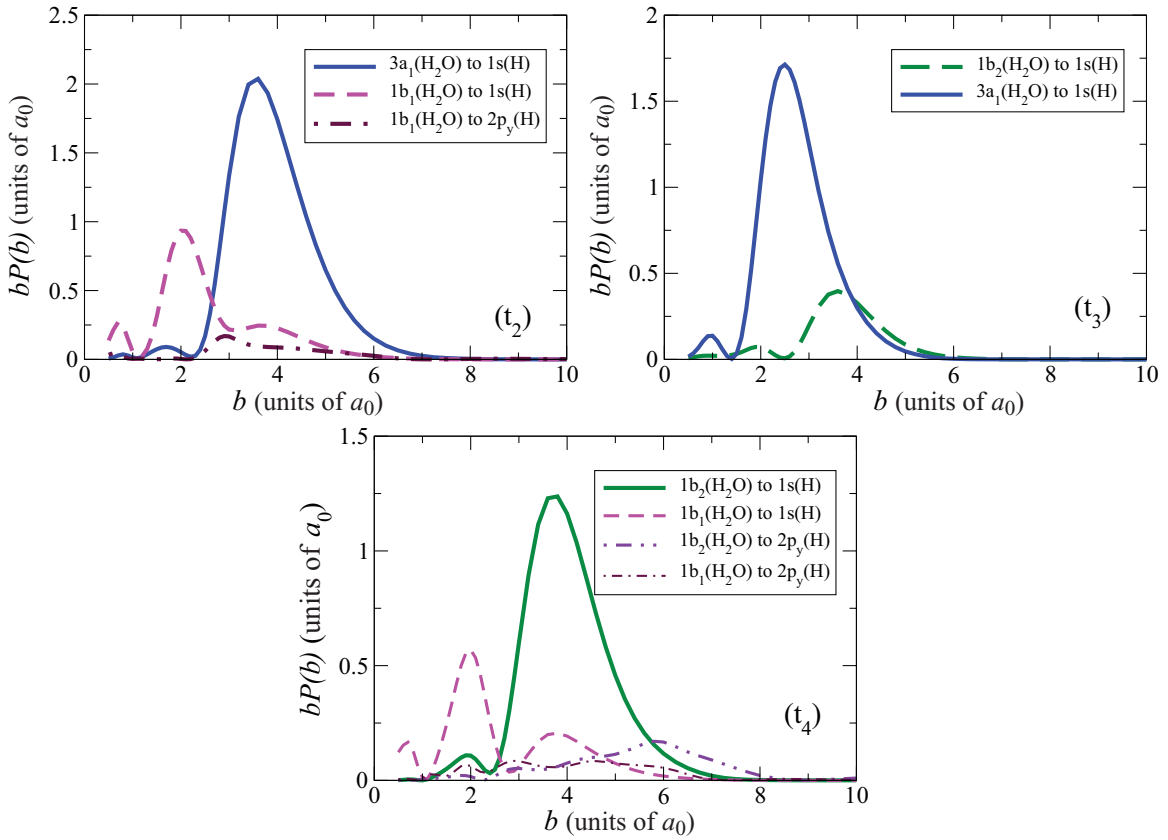

FIG. 5. (Color online) $bP(b)$ SEC transition probabilities for the three projectile trajectories indicated in the panels (t_2, t_3, and t_4) in $H^+ + H_2O$ collisions at 4 keV impact energy.

(see caption), at 4 keV impact energy, calculated using the MII. These figures confirm the need to consider the target anisotropy, given the strong relationship between the symmetry of the initial and final MOs and the projectile trajectory. For example, for t_2 and t_3 the transition with the highest probability is from $3a_1$ of H_2O to $1s$ of H, and for t_4 it is from $1b_2$ of H_2O to $1s$ of H. This figure also shows the impact parameters at which the function $bP(b)$ peaks ($b = 4a_0$ for t_2 and t_4, $b = 2.5a_0$ for t_3) and the magnitude of the peaks ($2.05a_0$ for t_2, $1.75a_0$ for t_3, and $1.25a_0$ for t_4) for these three trajectories. In the picture for t_4 trajectory, we can observe the low, but non-negligible, contribution of SEC transitions into H($2l$) energy levels to the total capture probabilities and, consequently, to the SEC cross sections.

F. Vibrational sudden approximation

Preliminary dynamical calculations in $H^+ + H_2O$ collisions have shown that SEC cross sections underestimate the experimental data for energies below 5–6 keV as a consequence of restricting our calculations to the Franck-Condon (FC) approximation of the molecule in its equilibrium geometry. In order to address this problem, we have used the vibrational-sudden approximation, performing dynamical calculations with a few distorted geometries of the water molecule.

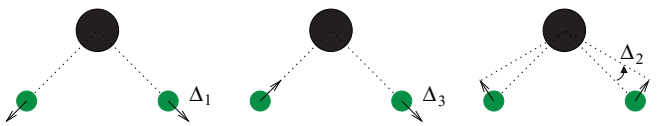

FIG. 6. (Color online) Vibrational modes for the water molecule: symmetric stretching A_1 (left), antisymmetric stretching B_2 (center), and bending A_1 (right).

In gas phase, the water molecule vibrations [34] involve combinations of the three vibrational modes shown in Fig. 6: symmetric stretching (left), antisymmetric stretching (center), and bending (right) of the covalent bonds. In order to choose several nuclear configurations to perform dynamical calculations, we have considered that the global zero point energy is $0.0410E_h$, with contributions from the symmetric stretching, antisymmetric stretching and bending modes of [35] $0.0166E_h$, $0.0171E_h$, and $0.007\,27E_h$, respectively.

To obtain the electronic energies for different molecular geometries, we have perform multireference configuration interaction (MRCI) calculations using a modified [36,37] MELD [38] package for each vibrational mode, as shown in Fig. 7: symmetric stretching (a), antisymmetric stretching (b), and bending (c). We then fitted these electronic energies to Morse potentials for the symmetric stretching,

$$V_s^M = -76.26 + 0.41\,(1 - e^{-1.24\,(\rho - 1.81)})^2, \qquad (38)$$

being $\rho = \rho_1 = \rho_2$ (see Table V caption) and bending,

$$V_\theta^M = -76.26 + 0.31\,(1 - e^{-0.018\,(\theta/2 - 53.04)}), \qquad (39)$$

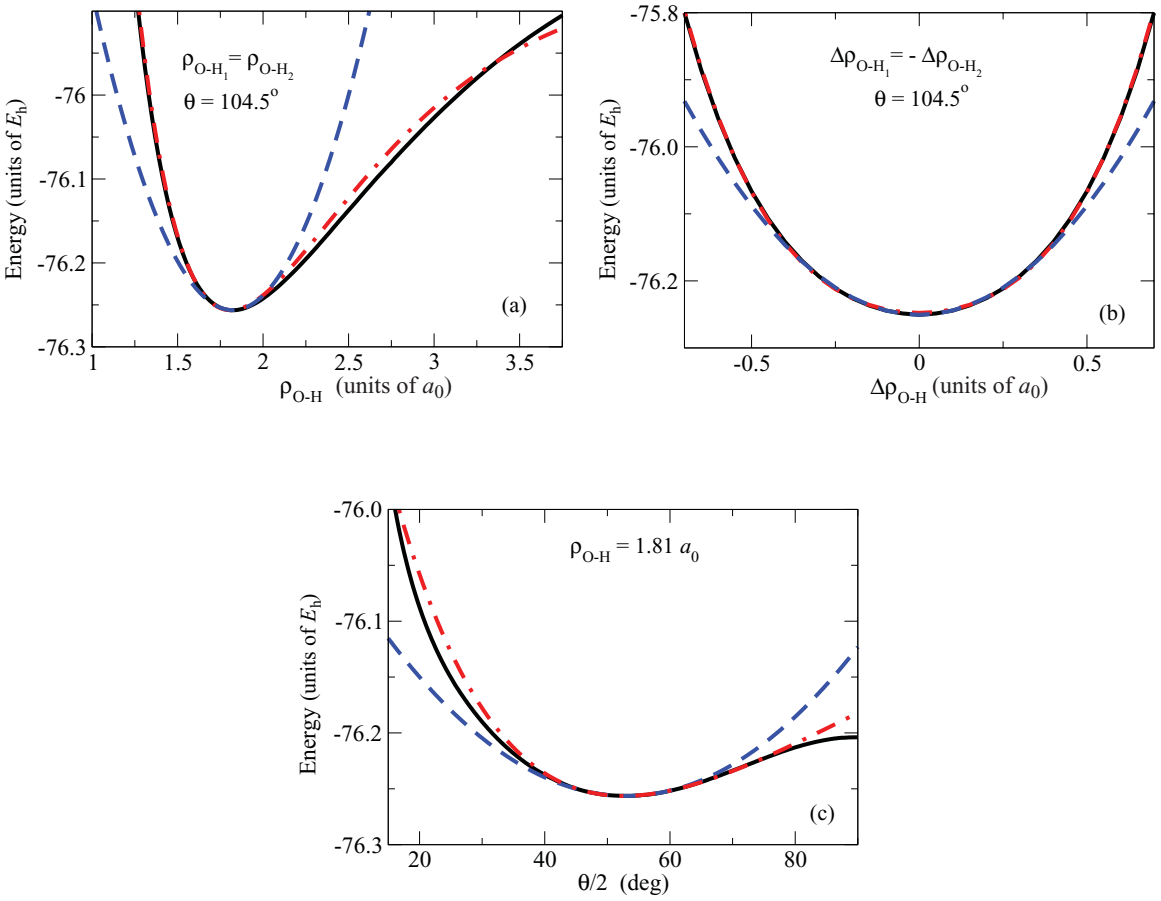

FIG. 7. (Color online) Water molecule electronic ground state potential energy curves obtained for the three vibrational modes sketched in Fig. 6. MRCI calculation (solid lines), fitted Morse [(a) and (c)] or quartic (b) potentials (dash-dotted lines), and fitted harmonic potentials (dashed lines). (a) Symmetric stretching A_1, (b) antisymmetric stretching B_2, (c) bending A_1.

θ also in Table V, and to a quartic type potential for antisymmetric stretching (just over the MRCI calculation),

$$V_a^C = -76.25 + 0.51\,\chi^2 + 0.83\,\chi^4, \qquad (40)$$

with $\chi = \rho_1 - \rho_0 = \rho_0 - \rho_2$ and ρ_0 the equilibrium O-H distance.

To get a small set of water molecule geometries that sufficiently sample its ground vibrational state, we have only consider geometries with an appreciable weight obtained from vibrational harmonic densities shown in Fig. 8.

TABLE V. Parameters of the seven different geometries employed to calculate $H^+ + H_2O$ cross sections using the sudden approximation and the weight for each geometry. $\theta = \widehat{HOH}$, ρ_1 = distance O-H_1, ρ_2 = distance O-H_2.

Geometry	θ (deg)	ρ_1 (a_0)	ρ_2 (a_0)	Weight
G_0^{eq}	104.5	1.81	1.81	0.4486
G_1	98.5	1.51	1.71	0.0821
G_2	110.5	1.61	1.61	0.0862
G_3	104.5	1.71	2.11	0.0851
G_4	98.5	2.01	2.01	0.0892
G_5	110.5	1.91	2.11	0.0821
G_6	104.5	1.61	1.61	0.1267

These densities have been obtained using the vibrational wave functions [39,40] of the harmonic potentials fitted to the set of three MRCI ones of Fig. 7. By employing a coordinate transformation to express these harmonic potentials as a function of the distortion from the equilibrium geometry, we can write the expressions for the symmetric stretching V_s^{harm}, bending V_θ^{harm}, and antisymmetric stretching

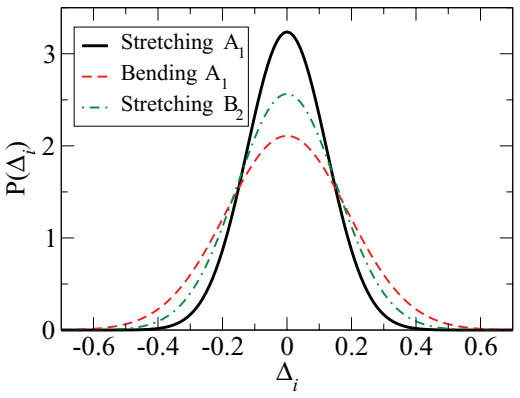

FIG. 8. (Color online) Probability density of the vibrational symmetry modes as a function of the displacements from the equilibrium geometry of H_2O, Δ_i, as illustrated in Fig. 6.

$V_a^{\rm harm}$ as

$$V_s^{\rm harm} = -76.26 + 0.056\,\Delta_1^2, \quad (41)$$

$$V_\theta^{\rm harm} = -76.26 + 9.7\times10^{-5}\,\Delta_2^2, \quad (42)$$

$$V_a^{\rm harm} = -76.25 + 0.65\,\Delta_3^2, \quad (43)$$

with Δ_1, Δ_2, and Δ_3 detailed in Fig. 6.

Once we get the probability for a given geometry, we can, with the fitted potentials from Fig. 7, obtain the corresponding electronic energies associated to the ground vibrational state ($0 \leqslant E_{\rm vib} \leqslant 0.06E_h$).

We have performed dynamical calculations for the distorted geometries given in Table V. Collisions performed using target molecules in nonequilibrium geometries can require additional relative projectile-target orientations (see previous section) to get the orientation-averaged cross sections. In the case of water collisions, 6 extra trajectories were employed to account for a total of 16 different ones, in calculations with geometries G_1, G_3, and G_5 listed in Table V.

To calculate the sudden orientation-averaged cross section, we use

$$\sigma^s = \sum_{k=0}^{6} \sigma_k W_k, \quad (44)$$

where σ_k is the orientation-averaged cross section for the water geometry k and W_k is the normalized weight of that geometry as given in Table V.

III. RESULTS AND DISCUSSION

A. $H^+ + H_2O$ collisions

In Fig. 9 we show the comparison between our SEC cross sections for impact energies in the range 1–110 keV, using MII (solid line in the figure), with several experimental data of [2,5–7], and with previous *ab initio* calculations performed by Mada *et al.* [12] and classical calculations by Illescas *et al.* [41]. Results of MII were obtained using the vibrational sudden approximation previously detailed and combining the results obtained with different values of the cutoff parameter η of Eq. (31): $\eta = 2$ for $E \leqslant 10$ keV and $\eta = 8$ for 10 keV

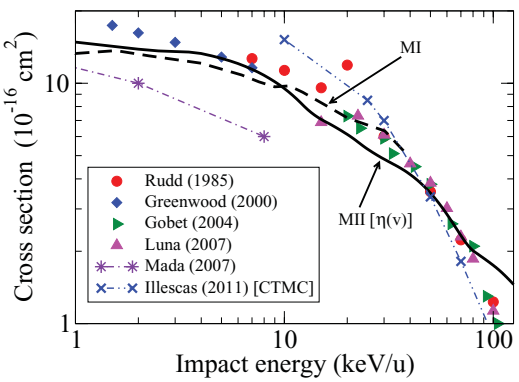

FIG. 9. (Color online) SEC cross section in $H^+ + H_2O$ collisions. Dashed line and solid line are the present results with Methods I and II, respectively. Star and cross symbols (with dot-dashed lines) correspond to other calculations and solid symbols correspond to experimental data, as indicated in the figure.

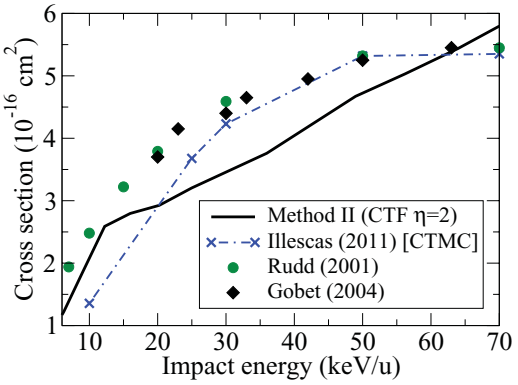

FIG. 10. (Color online) Single ionization cross section in $H^+ + H_2O$ collisions. The solid line is the present calculation with MII; the dot-dashed line is a CTMC calculation and the solid symbols correspond to experimental data, as indicated in the figure.

$\leqslant E \leqslant 30$ keV. For $E \geqslant 30$ keV we have employed, as an approximation to infinite values of η, an expansion of the wave function, in the set of asymptotic states, without translation factor; this accurately reproduces the experimental data for energies up to 100 keV.

We also show in Fig. 9 the results of MI within the FC approximation. In this case, given the more complete character of the basis employed, we have not introduced any TF. The results obtained with this method present a very good agreement with the experimental data for impact energies between 2 and 40 keV.

The calculations with MII for this system were made using 37 MOs [see Eq. (7)] to produce a total of 129 configurations [see Eq. (21)], of which 1 corresponds to the entrance channel, 24 account for electron capture to the projectile, 28 for ionization, and 76 for target excitation. We have not allowed transitions from the MO with lower energy ($1a_1$ of water) due to the large energy gap with other orbitals.

In Fig. 10, we show the SI cross-section calculated with MII. As ionization becomes important at higher energies, we have only performed FC calculations with $\eta = 2$. In this figure, we compare our results with two sets of experimental data [2,6] and with recent classical CTMC calculations [41]. Our results follow correctly the curve plotted by the experimental data for $E \leqslant 15$ keV, but slightly underestimate this data for higher energies, probably due to the limited number of ionization channels.

B. $He^{2+} + H_2O$ collisions

This system has been studied applying MII within the Franck-Condon approach, also using two values of the cutoff parameter $\eta = 2$, $\eta = 6$, and without CTF for impact energies higher than 10 keV, allowing us to make a fitting of these results from 0.4 to 70 keV.

Calculations for this system were performed using 37 MOs $\{\phi_i\}$ (7) to produce a total of 129 configurations $\{\Phi_j\}$ (21), of which 1 correspond to the entrance channel, 72 account for electron capture by the projectile, 12 for ionization, and 44 for target excitation. As in collisions with protons, we have not included transitions from the $1a_1$ MO of water to other orbitals.

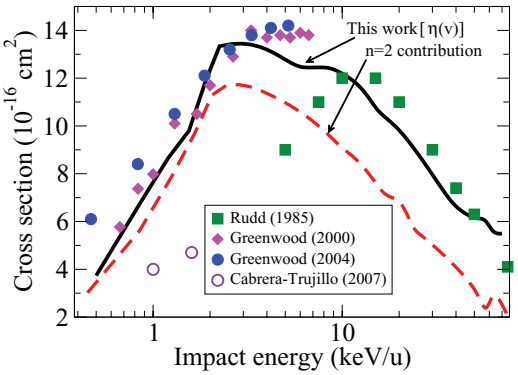

FIG. 11. (Color online) SEC cross section in $He^{2+} + H_2O$ collisions. The solid line is the present calculation with MII, the dashed line is the contribution to the SEC cross section from transitions to $n = 2$ of He^{2+}. Solid symbols correspond to experimental works as indicated in the figure.

In Fig. 11 we observe that our SEC cross sections compare well with experimental data of Refs. [2,5,42] (note the linear scale). The small differences at impact energies $E \leqslant 1.5$ keV/u are due to the use of the Franck-Condon approximation. Our SEC results improve previous theoretical results obtained using the electron-nuclear-dynamics *ab initio* calculations from Cabrera-Trujillo *et al.* [43].

The set of accurate $H^+ + H_2O$ and $He^{2+} + H_2O$ SEC cross sections in a wide range of impact energies ($0.5 \leqslant E \leqslant 100$ keV) is a consequence of two factors. The first one is the presence, in both systems, of an important set of pseudostates and excited states, which can absorb, in the first stages of the collision, the flux of electrons with positive energies, avoiding capture states of being contaminated by ionizing electrons. The second factor is the use of a cutoff parameter η that grows with the impact energy, making it possible to regularize the corrections to v^2 provided by the CTF method. These two factors permit to get SEC cross sections that accurately follow the experimental fall of the cross sections at increasing energies. In Fig. 12, we show the result for the $He^{2+} + H_2O$ system performed without a CTF. As it can be seen in the figure, the lack of a CTF for energies below 10 keV produces a clear underestimation of the experimental cross section. This behavior is also present in the $H^+ + H_2O$ system.

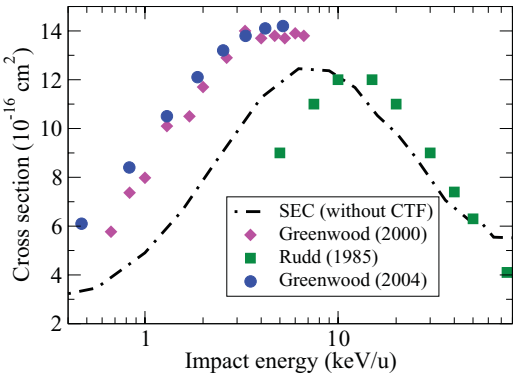

FIG. 12. (Color online) SEC cross section in $He^{2+} + H_2O$ collisions. The dash-dotted line is the present result with MII without CTF. Symbols are experimental data as indicated in the figure.

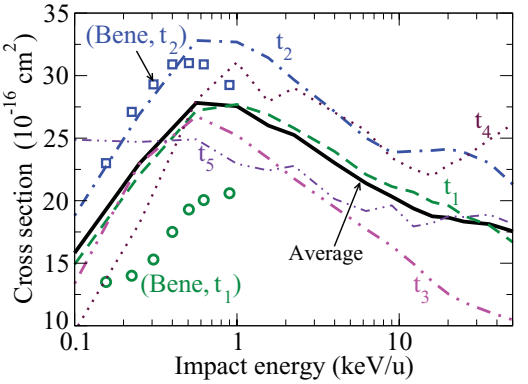

FIG. 13. (Color online) SEC cross section in $C^{2+} + CO$ collisions. Broken lines are the results obtained with the trajectory orientations of Fig. 2(b), as indicated in the figure. The solid line is the orientation-averaged result. The symbols are the calculations of Bene *et al.* [44] for the two trajectories indicated.

C. $C^{2+} + CO$ collisions

We have performed dynamical calculations expanding the wave function in a set of multielectronic configurations obtained using MII. This set includes the entrance channel $C^{2+}(^1S) + CO(^1\Sigma^+)$ and electron capture states as $C^+(^2P) + CO^+(^2\Sigma^+)$ and $C^+(^2P) + CO^+(^2\Pi^+)$, with the target CO molecule in its equilibrium geometry.

Method II calculations for this system were made using 23 MOs [see (7)] to produce a total of 71 configurations $\{\Phi_j\}$ (21), of which 1 is the entrance channel, 60 correspond to electron capture by the projectile, and the rest account for target excitation. In this system, we have allowed transitions from neither the two CO MOs with lowest energies due to the large energy gap to other MOs nor the $1s^2$ and $2s^2$ doubled occupy orbitals of the C^{2+} ion.

In Fig. 13 we present cross sections for $C^{2+}(^1S) + CO(^1\Sigma^+) \rightarrow C^+ + CO^+$ calculated for the five projectile trajectory types (broken lines: t_1 to t_5) sketched in Fig. 2(b).

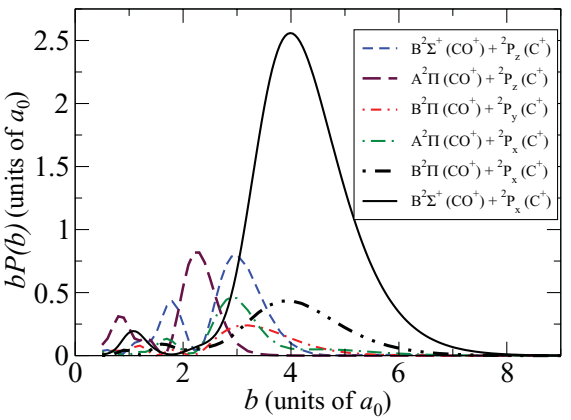

FIG. 14. (Color online) SEC transition probabilities $bP(b)$, as a function of the impact parameter b, for $C^{2+} + CO$ collisions along trajectories t_3 and with $E = 4$ keV.

The calculations of Bene *et al.* [44] (symbols) are presented for trajectories t_1 and t_2. We also provide orientation-averaged cross sections (solid line) for this system.

A good agreement is observed for trajectories t_2 at impact energies below their maximum (about 0.6 keV), while for trajectory t_1 the results of Bene *et al.* clearly fall below our values, which almost coincide with the orientation-averaged SEC cross section for all the range of impact energies considered.

As an illustration of the previously mentioned sensitivity of SEC transition probabilities to the projectile trajectory, we present in Fig. 14 the inelastic SEC transition probabilities $bP(b)$ as a function of impact parameter b, calculated for an impact energy of $E = 4$ keV along trajectory t_3, for different pairs of initial and final states. These curves show the strong relationship between geometries of initial and final states with the relative target-projectile orientation trajectories. In particular, C^{2+} t_3 trajectories favors transitions between $CO^+(B\,^2\Sigma^+)$ state to $C^+(^2p_x)$ orbital.

IV. CONCLUSIONS

We have performed semiclassical dynamical calculations using multicenter pseudopotentials to account for the interaction between active electrons and molecular cores, expanding the dynamical wave functions in terms of asymptotic dynamical orbitals in MI and in a set of multielectronic asymptotic configurations in MII. Transition probabilities have been obtained using the IEVM in MI to translate pseudopotentials monoelectronic probabilities to multielectronic ones. In MII, although transition probabilities are directly obtained from the dynamical coefficients, evaluation of multielectronic Hamiltonian matrix elements is approximated by using the IPM.

The implementation of the two simple methods MI and MII, based on the use of anisotropic pseudopotentials to describe the interaction of active electrons with ionic cores, has allowed us to extend the study of electron capture to the energy range between a few eV up to 100 keV. This has been possible partially because of the implementation of the vibrational-sudden approximation (in the $H^+ + H_2O$ system for MII at low energies) or the use of an almost complete basis set in MI. The use of a velocity-dependent cutoff (η) parameter has also allowed us to improve our results, in particular for intermediate energies, by the interpolation of the calculations obtained with different values of η.

To avoid the presence of divergent dynamical couplings in the abundant CIs loci, and the subsequent need of their regularization, we have employed nonadiabatic asymptotic MOs in both methods.

We have also analyzed, in detail, the electron capture process in the collisions $H^+ + H_2O$, $He^{2+} + H_2O$, and $C^{2+} + CO$, calculated using the previously detailed methods. Both $H^+ + H_2O$ and $He^{2+} + H_2O$ systems show good agreement with experimental data for the energy range between 1 and 80 keV.

Our results for $C^{2+} + CO$ collisions also show reasonable agreement with available theoretical calculations of [44] for two of the five types of trajectories. Experimental measurements of SEC cross sections for this system are necessary to check the accuracy of the calculated average cross section.

Although in this work we have concentrated in single-electron processes, the matrices **K** and **Z** described in the Appendix could be employed to study two-electron processes, which would allow to calculate transfer ionization, double ionization, double electronic target excitation, etc. In future works, we intend to improve MII to calculate cross sections for these processes.

ACKNOWLEDGMENTS

This work has been supported by DGICYT Project No. ENE2007-62934/FTN and by AIHH-HH2006-006-ESP-40/2006. Pablo M. M. Gabás also thanks MEC for the FPI grant to realize a short stay in Université Lyon I (2009) and Fundación Avelino López de Castro for a 3-month grant. The use of the computational facilities at the CCC of the Universidad Autónoma de Madrid is gratefully acknowledged.

APPENDIX: BUILDING CONFIGURATIONS IN METHOD II

To build the antisymmetric products of asymptotic orbitals in MII, we use the IPM approximation to calculate matrix elements between multielectronic configurations.

For the entrance channel we have

$$S_{11} = \langle \Psi_1 | \Psi_1 \rangle = 1, \tag{A1}$$

$$H_{11} = \langle \Psi_1 | H | \Psi_1 \rangle = \sum_{i=1}^{2j} \langle \Psi_1 | h_i | \Psi_1 \rangle \simeq 2 \sum_{i=1}^{j} h_{ii}, \tag{A2}$$

where j is the total number of valence MOs (5 for H_2O, 8 for CO). The matrix elements involving capture or excited states take the form

$$\begin{aligned} S_{pqrs}^{klmn} &= \langle \Psi_{km,ln} | \Psi_{pr,qs} \rangle \\ &= C_{klmnpqrs} \left(\left| Z_{pq}^{kl} \right| \left| Z_{rs}^{mn} \right| + \left| Z_{pq}^{mn} \right| \left| Z_{rs}^{kl} \right| \right), \end{aligned} \tag{A3}$$

$$\begin{aligned} H_{pqrs}^{klmn} &= \langle \Psi_{km,ln} | H | \Psi_{pr,qs} \rangle \\ &= C_{klmnpqrs} \left(\sum_{i=1}^{j} \left[\left| K_{pq}^{(i)kl} \right| \left| Z_{rs}^{mn} \right| + \left| Z_{pq}^{kl} \right| \left| K_{rs}^{(i)mn} \right| \right. \right. \\ &\quad \left. \left. + \left| K_{pq}^{(i)mn} \right| \left| Z_{rs}^{kl} \right| + \left| Z_{pq}^{mn} \right| \left| K_{rs}^{(i)kl} \right| \right] \right), \end{aligned} \tag{A4}$$

where the indexes *k, m, p*, and *r* indicate the valence MO, from which the electrons jump, and the indexes *l, n, q*, and *s* indicate the MO, to which the electrons go. Equations (A3) and (A4) are the most general expressions for matrix elements between different channels, including the entrance channel and several simple and double electron transition channels. The normalization coefficient $C_{klmnpqrs}$ depends on the specific process we are analyzing: single-electron transfer between the entrance channel and one excited electron configuration, transitions between two single excited electron states, between one excited electron state and two excited electrons state, also two-electron transitions between the entrance channel and doubly excited configurations, or transitions between doubly excited configurations.

The necessary matrices are

$$\mathbf{K}_{kl}^{(i)mn} = \begin{pmatrix} 1 & 0 & \dots & s_{1l} & \dots & 0 \\ 0 & 1 & \dots & s_{2l} & \dots & 0 \\ . & . & \dots & \dots & \dots & . \\ s_{m1} & s_{m2} & \dots & s_{ml} & \dots & s_{mj} \\ . & . & \dots & \dots & \dots & . \\ h_{i1} & h_{i2} & \dots & h_{il} & \dots & h_{ij} \\ . & . & \dots & \dots & \dots & . \\ 0 & 0 & \dots & s_{jl} & \dots & 1 \end{pmatrix}, \tag{A5}$$

and

$$\mathbf{Z}_{kl}^{mn} = \begin{pmatrix} 1 & 0 & \dots & s_{1l} & \dots & 0 \\ 0 & 1 & \dots & s_{2l} & \dots & 0 \\ . & . & \dots & \dots & \dots & . \\ s_{n1} & s_{n2} & \dots & s_{nl} & \dots & s_{nj} \\ . & . & \dots & \dots & \dots & . \\ 0 & 0 & \dots & s_{jl} & \dots & 1 \end{pmatrix}. \tag{A6}$$

The $\mathbf{Z}_{kl}^{mn}$ matrix is obtained from the unit matrix by replacing the elements of column k by the corresponding column l from the monoelectronic **s** matrix and the elements of the m row with the corresponding n row from the monoelectronic **s** matrix. The $\mathbf{K}_{kl}^{(i)mn}$ matrix is obtained from the unit matrix by replacing the elements of the k column by those coming from the l column of the monoelectronic **s** matrix, and the elements of the m row with the elements of the n row of the **s** matrix, and the elements of the i row by those of the i row of the monoelectronic Hamiltonian **h** matrix.

[1] R. Dagnac, D. Blanc, and D. Molina, J. Phys. B **3**, 1239 (1970).
[2] M. E. Rudd, T. V. Goffe, R. D. DuBois, and L. H. Toburen, Phys. Rev. A **31**, 492 (1985).
[3] M. A. Bolorizadeh and M. E. Rudd, Phys. Rev. A **33**, 888 (1986).
[4] U. Werner, K. Beckord, J. Becker, and H. O. Lutz, Phys. Rev. Lett. **74**, 1962 (1995).
[5] J. B. Greenwood, A. Chutjian, and S. J. Smith, Astrophys. J. **529**, 605 (2000).
[6] F. Gobet *et al.*, Phys. Rev. A **70**, 062716 (2004).
[7] H. Luna *et al.*, Phys. Rev. A **75**, 042711 (2007).
[8] Belkić, J. Math. Chem. **47**, 1366 (2010).
[9] B. Gervais, M. Beuve, G. H. Olivera, and M. E. Galassi, Radiat. Phys. Chem. **75**, 493 (2006).
[10] O. Boudrioua, C. Champion, C. DalCappello, and Y. V. Popov, Phys. Rev. A **75**, 022720 (2007).
[11] L. F. Errea, C. Illescas, L. Méndez, B. Pons, I. Rabadán, and A. Riera, Phys. Rev. A **76**, 040701 (2007).
[12] S. Mada, K. N. Hida, M. Kimura, L. Pichl, H.-P. Liebermann, Y. Li, and R. J. Buenker, Phys. Rev. A **75**, 022706 (2007).
[13] L. F. Errea, A. Macías, L. Méndez, I. Rabadán, A. Riera, A. Rojas, and P. Sanz, Phys. Rev. A **63**, 062713 (2001).
[14] G. Horneck and P. Rettberg, *Complete Course in Astrobiology* (Wiley-VCH, Berlin, 2007).
[15] P. D. Fainstein, G. H. Olivera, and R. D. Rivarola, Nucl. Instrum. Methods B **107**, 19 (1996).
[16] L. Wu and R. Wang, Pharmacol. Rev. **57**, 585 (2005).
[17] M. C. Bacchus-Montabonel, M. Łabuda, Y. S. Tergiman, and J. E. Sienkiewicz, Phys. Rev. A **72**, 052706 (2005).
[18] M. C. Bacchus-Montabonel and Y. S. Tergiman, Phys. Rev. A **74**, 054702 (2006).
[19] M. C. Bacchus-Montabonel, Y. S. Tergiman, and D. Talbi, Phys. Rev. A **79**, 012710 (2009).
[20] I. Rabadán, L. F. Errea, P. Martínez, and L. Méndez, AIP Conf. Proc. **1080**, 98 (2008).
[21] L. F. Errea, L. Méndez, and A. Riera, J. Phys. B **15**, 101 (1982).
[22] B. H. Bransden and M. H. C. McDowell, *Charge Exchange and the Theory of Ion-Atom Collisions* (Oxford, Clarendon, 1992).
[23] P. O. Widmark, P. Malmqvist, and B. Roos, Theor. Chim. Acta **77**, 291 (1990).
[24] See Supplemental Material at http://link.aps.org/supplemental/10.1103/PhysRevA.85.012702 for our basis for the hydrogen atom.
[25] See Supplemental Material at http://link.aps.org/supplemental/10.1103/PhysRevA.85.012702 for our basis for helium atom.
[26] See Supplemental Material at http://link.aps.org/supplemental/10.1103/PhysRevA.85.012702 for our basis for oxygen atom.
[27] D. S. F. Crothers and R. McCarroll, J. Phys. B **20**, 2835 (1987).
[28] R. K. Janev, E. A. Solov'ev, and D. Jakimovski, J. Phys. B **28**, L615 (1995).
[29] L. Errea, J. D. Gorfinkiel, C. Harel, H. Jouin, A. Macías, L. Méndez, B. Pons, and A. Riera, J. Phys. B **33**, 3107 (2000).
[30] W. R. Thorson and J. B Delos, Phys. Rev. A **18**, 117 (1978).
[31] L. F. Errea, C. Harel, H. Jouin, L. Méndez, B. Pons, and A. Riera, J. Phys. B **27**, 3603 (1994).

[32] L. F. Errea, A. Macías, L. Méndez, I. Rabadán, A. Riera, and A. Rojas, Phys. Scr. **T92**, 202 (2001).
[33] G. B. Arfken and H. J. Webber, *Mathematical Methods for Physicist* (Harcourt, San Diego, 2005).
[34] R. Lemus, J. Mol. Spectrosc. **225**, 73 (2004).
[35] D. Eisenberg and W. Kauzmann, *The Structure and Properties of Water* (Oxford university Press, London, 1969).
[36] L. F. Errea, A. Macías, L. Méndez, I. Rabadán, and A. Riera, J. Phys. B **33**, L615 (2000).
[37] J. F. Castillo, L. F. Errea, A. Macías, L. Méndez, and A. Riera, J. Chem. Phys. **103**, 2113 (1995).
[38] E. R. Davidson, in MOTECC, *in Modern Techniques in Computational Chemistry*, edited by E. Clementi (ESCOM, Leiden, 1990).
[39] E. B. Wilson, J. C. Decius, and P. C. Cross, *Molecular Vibrations: The Theory of Infrared and Ramman Vibrational Spectra* (Courier Dover Publications, Mineola, NY, 1955).
[40] P. W. Atkins, *Physical chemistry* (Oxford University Press, Oxford, 1998).
[41] C. Illescas, L. F. Errea, L. Méndez, B. Pons, I. Rabadán, and A. Riera, Phys. Rev. A **83**, 052704 (2011).
[42] J. B. Greenwood, R. J. Mawhorter, I. Čadež, J. Lozano, S. J. Smith, and A. Chutjian, Phys. Scr. **T110**, 358 (2004).
[43] R. Cabrera-Trujillo, E. Deumens, Y. Ohrn, O. Quinet, J. R. Sabin, and N. Stolterfoht, Phys. Rev. A **75**, 052702 (2007).
[44] E. Bene, P. Martínez, G. J. Halsáz, A. Vibók, and M. C. Bacchus-Montabonel, Phys. Rev. A **80**, 012711 (2009).